



FORCE-VIBRATION TESTING OF BUILDINGS USING THE LINEAR SHAKER SEISMIC SIMULATION (LSSS) TESTING METHOD

Eunjong YU¹, Daniel H. WHANG², Ravi VENUGOPAL³, Jonathan P. STEWART⁴
and John. W. WALLACE⁴

SUMMARY

This paper describes the development and numerical verification of a test method to realistically simulate the seismic structural response of full-scale buildings. The result is a new field testing procedure referred to as the linear shaker seismic simulation (LSSS) testing method. This test method uses a linear shaker system in which a mass mounted on the structure is commanded to follow a specified acceleration response history, which in turn induces inertial forces in the structure. The inertia force of the moving mass is transferred as dynamic force excitation to the structure. The key issues associated with the LSSS method are (1) determining for a given ground motion displacement, x_g , a linear shaker motion which induces a structural response that matches as closely as possible the response of the building if it had been excited at its base by x_g (i.e., the motion transformation problem) and (2) correcting the linear shaker motion from Step 1 to compensate for control-structure interaction (CSI) effects associated with the fact that linear shaker systems cannot impart perfectly to the structure the specified forcing functions (i.e., the CSI problem). The motion transformation problem is solved using filters that modify x_g both in the frequency domain using building transfer functions and in the time domain using a least squares approximation. The CSI problem, which is most important near the modal frequencies of the structural system, is solved for the example of a linear shaker system that is part of the nees@UCLA equipment site.

INTRODUCTION

Field performance data from full-scale structural systems have been a principal driving force behind advances in earthquake engineering practice since the early 20th century. For example, observations of structural collapse following the 1933 Long Beach earthquake led to some of the first formal recommendations on earthquake resistant design and retrofitting of existing structures [1]. More recently, observations of building performance following the 1971 San Fernando, 1989 Loma Prieta and 1994 Northridge earthquakes provided the impetus for major building code revisions in the 1976, 1985, 1991 and 1997 versions of the Uniform Building code. The weight given to field performance data stems from

¹ Graduate student, University of California, Los Angeles, Email: eunjong@ucla.edu

² Assistant Research Engineer, University of California, Los Angeles

³ Founder and Senior Consulting Engineer, Sysendes, Inc., Montréal, Canada

⁴ Associate Professor, University of California, Los Angeles

a simple fact: it represents the “ground truth” information against which all analysis procedures, code provisions, and other tests results must be calibrated.

Field performance data in structures can be generated either by seismic excitation or forced vibration testing. The focus here is on forced vibration testing of full scale structures. Advantages of field testing relative to laboratory testing include the lack of need for scaling, correct boundary conditions, and correct modeling of system interactions. However, several factors have limited the impact of field testing to date, including:

1. The inability of artificial (forced) vibration sources to test structures at large amplitudes, in particular, into the nonlinear range.
2. The inability of traditional vibration sources to excite structures in a manner that emulates realistic broadband seismic excitation.
3. Practical difficulties associated with deploying a sufficiently dense sensor array such that detailed component behavior can be investigated.

The NSF-funded George E. Brown, Jr. Network for Earthquake Engineering Simulation (NEES) project at UCLA is addressing each of these issues by developing large capacity harmonic eccentric shakers, a linear shaker able to reproduce broadband seismic excitation, and a field data acquisition system with IP-based wireless telemetry that enables convenient deployment of large sensor arrays.

This paper focuses on the second issue identified above: the development of a linear broadband shaker system to provide structural excitations that realistically simulate linear elastic structural seismic response. The theoretical framework for the proposed test method is developed and illustrated with a numerical example. The result is a new field testing procedure referred to as the linear shaker seismic simulation (LSSS) testing method. LSSS represents a fifth type of test method to investigate the dynamic response of structural systems; the other methods being quasi-static cyclic, pseudodynamic, shake table and effective force testing [2].

DESCRIPTION OF THE LSSS METHOD

During an earthquake, a building is subjected to inertial forces caused by a ground motion (x_g). As shown in Fig. 1(a), the effect of base excitation on a building is equivalent to that of a set of effective earthquake lateral forces applied to the building on a stationary base. These effective earthquake forces depend on the building inertia properties and the earthquake ground acceleration. In contrast, force-vibration experiments are typically designed such that the mechanical shakers are anchored to the roof or some other level of the test structure. Consequently, vibrations induced during force-vibration experiments and earthquakes emanate from opposite locations – “top excitation” during force-vibration experiments and “base excitation” during earthquakes. Hence, the lateral force distributions induced during the two cases are different since the linear shaker can only apply an inertial force to the floor where it is attached. This difference can be described in terms of the influence vector, \underline{l} , which defines the degrees-of-freedom affected by the external excitation as follows:

$$\underline{f}(t) = -\mathbf{M} \underline{l} \ddot{x}_a(t) \quad (1)$$

where, $\underline{f}(t)$ = effective lateral force vector, \mathbf{M} = mass matrix of the building, $\underline{l} = (n \times 1)$ influence vector, $\ddot{x}_a(t)$ = applied acceleration history due to either the ground motion ($\ddot{x}_a(t) = \ddot{x}_g(t)$) or shaker excitation ($\ddot{x}_a(t) = \ddot{x}_{sa}(t)$, where $\ddot{x}_{sa}(t)$ = absolute shaker acceleration), and n = number of dynamic degrees-of-freedom in the building. The difference in the \underline{l} vectors for the base and top excitation cases is illustrated in Fig. 1 for a 3-story building model with one translational degree-of-freedom per floor.

In Fig. 1 and Eq. (1), $x_{sa}(t)$ is the absolute displacement of the moving mass m_s of the linear shaker, and m_i is the mass of floor level i in the building. The displacement $x_{sa}(t)$ is distinguished in Fig. 2 from the displacement of the roof relative to the base $x_n(t)$ and the displacement of the shaker mass relative to the roof $x_s(t)$.

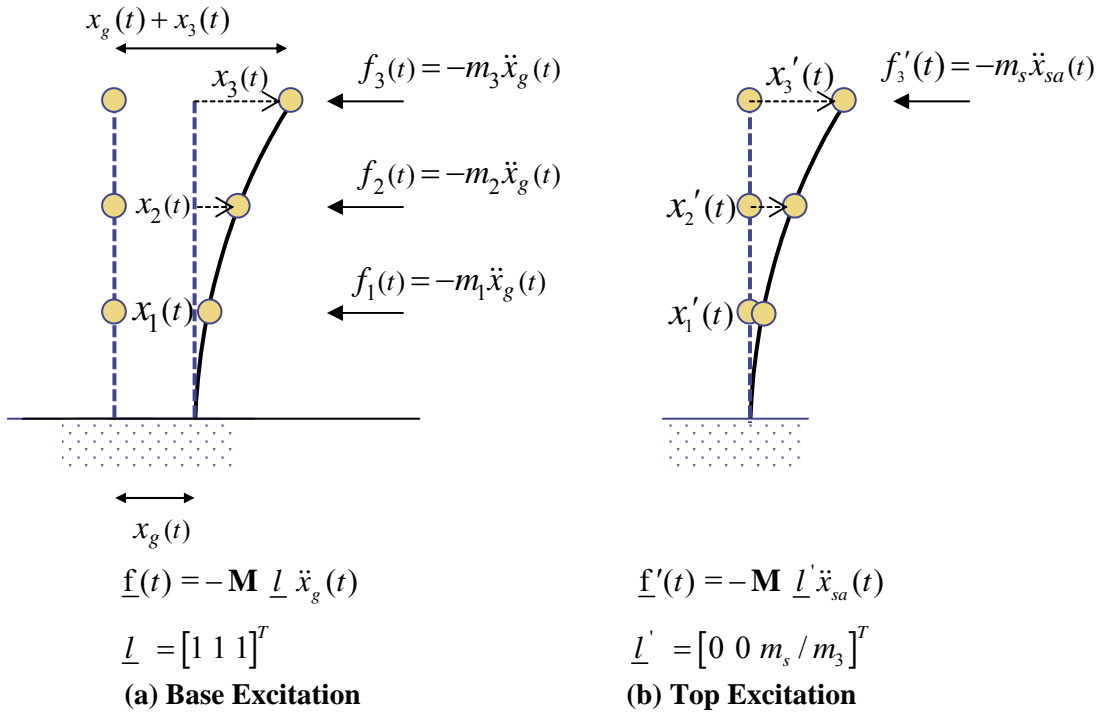


Fig. 1. Comparison of effective force distributions for earthquake excitation and shaker excitation

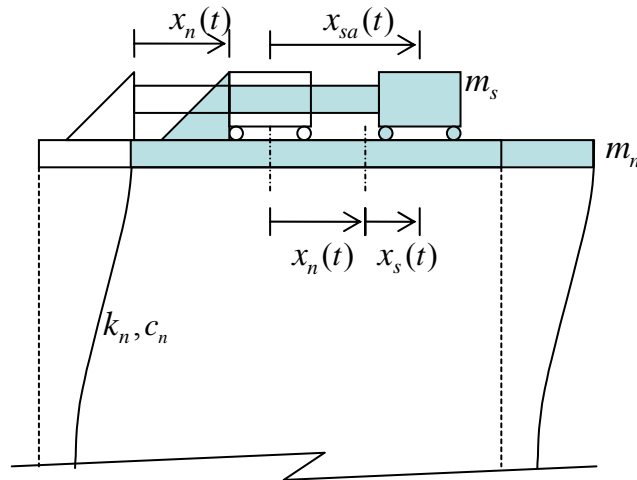


Fig. 2. Coordinate system for linear shaker on a test structure

Clearly, if the same acceleration history was applied for the base and top excitation cases (i.e., $\ddot{x}'_{sa}(t) = \ddot{x}_g(t)$), different structural responses would be induced. Accordingly, the first major challenge associated with the development of the LSSS testing method is to determine for a given ground motion, $x_g(t)$, a linear shaker input motion which induces a structural response that matches as closely as possible (in the linear elastic range) the response of the building if it had been excited at its base by $x_g(t)$. Two alternative solutions to this motion transformation problem are presented. The first approach filters the ground motion $x_g(t)$ in the frequency domain using building transfer functions, while the second approach modifies the forcing function in the time domain using a least squares approximation. Both of the motion transformation methods assume that the linear shaker can reproduce the specified forcing function exactly

(i.e., perfect control system). As shown later, this assumption is not always realistic. For example, experimental studies by Dyke et al. [3] and Dimig et al. [2] have shown that servo-hydraulic actuators attached to lightly damped structures are limited in their ability to apply forces near the test structure's natural frequencies. Consequently, the second challenge in developing the LSSS test method is to account for imperfect hydraulic actuator control by pre-correcting the shaker input motion that would be obtained under the assumption of a perfect control system (i.e., the control-structure interaction problem). In the following sections, mathematical solutions to the motion transformation and control-structure interaction problems are described.

THE MOTION TRANSFORMATION PROBLEM

LSSS Transfer Function Method

The equation of motion of an elastic n degrees-of-freedom building structure subjected to a lateral force vector $\underline{f}(t)$ can be expressed as

$$\mathbf{M}\ddot{\underline{x}}(t) + \mathbf{C}\dot{\underline{x}}(t) + \mathbf{K}\underline{x}(t) = \underline{f}(t) \quad (2)$$

where, $\underline{x}(t) = (n \times 1)$ displacement vector relative to the base, \mathbf{M} , \mathbf{C} and, $\mathbf{K} = (n \times n)$ mass, damping and stiffness matrices, respectively. Assuming zero initial conditions, the Laplace transformation of Eq. (2) yields,

$$[\mathbf{M}s^2 + \mathbf{C}s + \mathbf{K}] \underline{x}(s) = \underline{f}(s) \quad (3)$$

in which s denotes the Laplace domain parameter. The $(n \times n)$ transfer function matrix $\mathbf{H}(s)$ transforms the input forcing function $\underline{f}(s)$ into the output vector $\underline{x}(s)$, i.e.,

$$\underline{x}(s) = \mathbf{H}(s) \underline{f}(s) \quad (4)$$

A unique transfer function exists for the output (displacement) at the i -th DOF due to the input (force) at the j -th DOF, which is represented by the $H_{ij}(s)$ component of $\mathbf{H}(s)$. Using Eq. (4), the dynamic response of a linear elastic structure can be derived using the inverse Laplace transformation of $\underline{x}(s)$,

$$\underline{x}(t) = L^{-1}\{\underline{x}(s)\} = L^{-1}\{\mathbf{H}(s) \underline{f}(s)\} \quad (5)$$

Since the displacement response of the i -th floor (x_i) is the superposition of the responses associated with inputs applied at each floor, displacement x_i can be expressed by the sum of the transfer functions and inputs at each floor. Representing the input by equivalent lateral force vectors $\underline{f}(t)$ (e.g., Fig. 1), displacement responses x_i and x_i' for base and top excitation, respectively, are given by:

$$\text{Base excitation: } x_i(s) = \sum_{j=1}^n H_{ij}(s) f_j(s) = - \sum_{j=1}^n H_{ij}(s) m_j \ddot{x}_g(s) \quad (6)$$

$$\text{Top excitation: } x_i'(s) = \sum_{j=1}^n H_{ij}(s) f_j'(s) = - \sum_{j=1}^n H_{ij}(s) m_j l_j' \ddot{x}_{sa}(s) \quad (7)$$

where, f_j and m_j represent effective earthquake force and story mass at floor j , $\ddot{x}_g(s)$ is the Laplace transformation of the ground motion, and l_j' is the j -th components of influence vector \underline{l}' . For the special case of excitation applied only at the roof level (i.e., $j = n$ only), Eq. (7) reduces to

$$x_i'(s) = -H_{in}(s) m_s \ddot{x}_{sa}(s) \quad (8)$$

where, H_{in} is the transfer function between the shaker input on floor level n and the displacement response of the i -th floor. Equating Eqs. (6) and (8), the linear shaker input motion $\ddot{x}_{sa}(s)$ that will

induce an i -th floor response, $x_i'(s)$, that will match $x_i(s)$ from the base excitation can be derived using a filter $T(s)$ defined as

$$T(s) = \frac{\sum_{j=1}^n H_{ij}(s)m_j}{H_{in}(s)m_s} \quad (9)$$

Finally, the shaker input motion \ddot{x}_{sa} is obtained using as

$$\ddot{x}_{sa}(t) = L^{-1} \{ \ddot{x}_{sa}(s) \} = L^{-1} \{ T(s) \ddot{x}_g(s) \} \quad (10)$$

In this approach, the shaker input motion $\ddot{x}_{sa}(t)$ is obtained through a filter defined as the ratio of two transfer functions such that the responses of the i -th floor due to the base excitation and top excitations will coincide. Note that $T(s)$ depends on which aspect (DOF) of the response is being matched. This method can be extended to replicate alternative response quantities such as total base shear, story overturning moment, or inter-story drift. However, a shortcoming of this approach is its inability to match simultaneously the response of multiple DOFs (or multiple response quantities).

LSSS Least Squares Method

From the governing equation of the MDOF dynamic system response subjected to base excitation (Eq. 2), the discrete form of the solution can be found using the Newmark explicit method [4] as follows:

$$\underline{x}(k+1) = \underline{x}(k) + \Delta t \underline{\dot{x}}(k) + \frac{1}{2} \Delta t^2 \underline{\ddot{x}}(k) \quad (11a)$$

$$\underline{\dot{x}}(k+1) = \underline{\dot{x}}(k) + \frac{1}{2} \Delta t [\underline{\ddot{x}}(k) + \underline{\ddot{x}}(k+1)] \quad (11b)$$

Substituting Eqs. (11) into Eq.(2), and introducing the structural response vector, \underline{z} , results in the following discrete state equation [5]:

$$\underline{z}(k+1) = \mathbf{A} \underline{z}(k) + \underline{L} \ddot{x}_g(k+1) \quad (12)$$

where

$$\underline{z}(k) = \begin{bmatrix} \underline{x}(k) \\ \Delta t \underline{\dot{x}}(k) \\ \Delta t^2 \underline{\ddot{x}}(k) \end{bmatrix} \quad (13a)$$

$$\mathbf{A} = \begin{bmatrix} \mathbf{I} & \mathbf{I} & \frac{1}{2} \mathbf{I} \\ -\frac{1}{2} \Delta t^2 \hat{\mathbf{M}}^{-1} \mathbf{K} & \mathbf{I} - \frac{1}{2} [\Delta t \hat{\mathbf{M}}^{-1} \mathbf{C} + \Delta t^2 \hat{\mathbf{M}}^{-1} \mathbf{K}] & \frac{1}{2} [\mathbf{I} - \frac{1}{2} \Delta t \hat{\mathbf{M}}^{-1} \mathbf{C}] - \frac{1}{4} \Delta t^2 \hat{\mathbf{M}}^{-1} \mathbf{K} \\ -\Delta t^2 \hat{\mathbf{M}}^{-1} \mathbf{K} & -\Delta t \hat{\mathbf{M}}^{-1} \mathbf{C} - \Delta t^2 \hat{\mathbf{M}}^{-1} \mathbf{K} & -\frac{1}{2} \Delta t \hat{\mathbf{M}}^{-1} \mathbf{C} - \frac{1}{2} \Delta t^2 \hat{\mathbf{M}}^{-1} \mathbf{K} \end{bmatrix} \quad (13b)$$

$$\underline{\mathbf{L}} = \begin{bmatrix} \underline{\mathbf{0}} \\ \frac{1}{2} \Delta t^2 \hat{\mathbf{M}}^{-1} \mathbf{M} \underline{\mathbf{l}} \\ \Delta t^2 \hat{\mathbf{M}}^{-1} \mathbf{M} \underline{\mathbf{l}} \end{bmatrix} ; \quad \hat{\mathbf{M}} = \mathbf{M} + \frac{1}{2} \mathbf{C} \Delta t \quad (13c), (13d)$$

In the above equations, Δt is the constant time step, \mathbf{I} is the $(n \times n)$ identity matrix, $\ddot{x}_g(k+1)$ is the ground acceleration at discrete time $t = (k+1)\Delta t$, and $\underline{\mathbf{0}}$ is an $(n \times 1)$ vector of zeros. Column vector $\underline{\mathbf{z}}(k)$ is referred to as the structural response vector at discrete time $t = k\Delta t$ and has length $3n$, as does vector $\underline{\mathbf{L}}$. The response of the structure subjected to top excitation can be expressed similarly as

$$\underline{\mathbf{z}}'(k+1) = \mathbf{A} \underline{\mathbf{z}}(k) + \underline{\mathbf{L}}' \ddot{x}_{sa}(k+1) \quad (14)$$

where $\underline{\mathbf{z}}'(k+1)$ and $\ddot{x}_{sa}(k+1)$ represent the structural response vector and shaker acceleration at time $k+1$ in the case of top excitation, and $\underline{\mathbf{L}}'$ is determined using the influence vector $\underline{\mathbf{l}}'$ instead of $\underline{\mathbf{l}}$ in Eq. (13c). System matrix \mathbf{A} has dimensions of $3n \times 3n$ and is identical for both the base and top excitation cases. Since the response of the system at time N is the superposition of the responses to the individual inputs at time $t = 0, 1, \dots, N$, the difference in the structural response between base and top excitation cases at time step $t = N$ can be expressed as:

$$\underline{\boldsymbol{\varepsilon}}(N) = \underline{\mathbf{z}}(N) - \underline{\mathbf{z}}'(N) = \underline{\mathbf{z}}(N) - \left[(\mathbf{A})^N \mathbf{L}' \ddot{x}_{sa}(0) + (\mathbf{A})^{N-1} \mathbf{L}' \ddot{x}_{sa}(1) + \dots + \mathbf{L}' \ddot{x}_{sa}(N) \right] \quad (15)$$

The error vector $\underline{\boldsymbol{\varepsilon}}$ is then introduced as:

$$\underline{\boldsymbol{\varepsilon}} = \begin{Bmatrix} \underline{\boldsymbol{\varepsilon}}(1) \\ \underline{\boldsymbol{\varepsilon}}(2) \\ \vdots \\ \underline{\boldsymbol{\varepsilon}}(N) \end{Bmatrix} = \begin{Bmatrix} \underline{\mathbf{z}}(1) \\ \underline{\mathbf{z}}(2) \\ \vdots \\ \underline{\mathbf{z}}(N) \end{Bmatrix} - \begin{bmatrix} \mathbf{L}' & \mathbf{0} & \dots & \mathbf{0} \\ \mathbf{A}\mathbf{L}' & \mathbf{L}' & \dots & \mathbf{0} \\ \vdots & \vdots & \ddots & \vdots \\ (\mathbf{A})^{N-1} \mathbf{L}' & (\mathbf{A})^{N-2} \mathbf{L}' & \dots & \mathbf{L}' \end{bmatrix} \begin{Bmatrix} \ddot{x}_{sa}(1) \\ \ddot{x}_{sa}(2) \\ \vdots \\ \ddot{x}_{sa}(N) \end{Bmatrix} \quad (16a)$$

or

$$\underline{\boldsymbol{\varepsilon}} = \underline{\mathbf{z}} - \mathbf{G} \underline{\ddot{x}}_{sa} \quad (16b)$$

where the dimensions of $\underline{\boldsymbol{\varepsilon}}$, $\underline{\mathbf{z}}$, \mathbf{G} , and $\underline{\ddot{x}}_{sa}$ are $(3nN \times 1)$, $(3nN \times 1)$, $(3nN \times N)$, and $(N \times 1)$, respectively. Therefore, the linear shaker input motion $\underline{\ddot{x}}_{sa}$ which minimizes the error between $\underline{\mathbf{z}}$ and $\underline{\mathbf{z}}'$ can be derived by minimizing the L_2 norm of the errors from time $t=1$ to N . A closed form solution can be found using the least squares method.

$$\underline{\ddot{x}}_{sa} = (\mathbf{G}^T \mathbf{G})^{-1} \mathbf{G}^T \underline{\mathbf{z}} \quad (17)$$

The LSSS least squares method differs from the transfer function approach in that the least squares approach minimizes the error for the displacement, velocity, and acceleration responses at all DOFs simultaneously. Furthermore, the least squares method can be extended to nonlinear response problems provided that the nonlinear properties of the structure are known. However, applications to nonlinear systems are beyond the scope of this paper.

THE CONTROL-STRUCTURE INTERACTION PROBLEM

Dyke et al. (1995) found that the natural velocity feedback loop that exists in hydraulic actuators can cause dynamic coupling between the test structure and actuator. This feedback loop results from the imperfect ability of the control system (e.g., controller, servo-valve, and actuator) to provide hydraulic fluid to the piston chamber as the piston displaces. This effect is accentuated when displacements of the

piston are large, which occur near the natural frequencies of the test structure. Accordingly, this dynamic coupling effect, termed control-structure interaction (CSI), can restrict the ability of hydraulic actuators to apply forces near the natural frequencies of the structure. When CSI effects are uncompensated for, they can cause significant discrepancies between the desired and achieved system response [2].

Linearized model of servo-hydraulic actuator and test structure

A linearized model of both the servo-hydraulic actuator system and the structure to which it is attached was developed as shown in Fig. 3. While the model is fully general, it is customized here to simulate the performance of the UCLA NEES servo-hydraulic linear shaker attached to a test structure. Although servo-hydraulic actuation is an inherently nonlinear process, a linearized model was used since it has been shown to capture the salient features of the dynamic interactions of the overall system [6]. The block diagram in Fig. 3 includes an idealized uni-axial, displacement controlled linear shaker system along with a test structure. The overall system described in Fig. 3 consists of several subsystems that are subject to various types of feedback loops as follows:

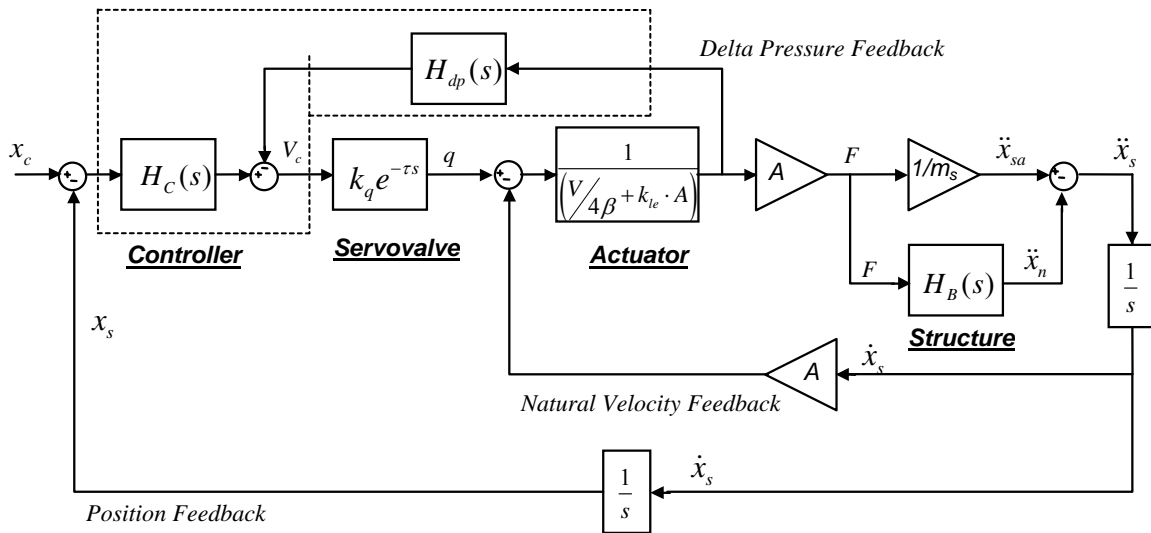


Fig. 3. Block diagram model of structure-servo hydraulic shaker system

- Natural velocity feedback: The structure displaces when a force is applied by the actuator. Since the actuator cylinder is fixed to the floor of the test building, the movement of the structure/floor results in additional relative displacement between the actuator cylinder and the actuator piston (see Fig. 2). This additional movement induces a volume change in both sides of the actuator chamber, thereby resulting in a change in the differential oil pressure across the piston from the command. This change in oil pressure, which causes a deviation of the achieved force and displacement from the target values, is referred to as natural velocity feedback. The natural velocity feedback is an inherent feature of the linear shaker-structure system, but is dependent on the control algorithm of the hydraulic system.
- Position feedback: The actuator piston movement caused by the action of the combined controller-servovalve-actuator-structure system is monitored (as either a displacement, velocity, or acceleration) and is fed back to the controller so that adjustments can be made if the measured response (x_s) does not match the commanded shaker input motion (x_c). The natural velocity feedback is an important contributor to the difference between x_s and x_c .
- Delta pressure feedback: The displacement of the piston relative to the actuator cylinder occurs due to the pressure differential across the piston. The pressure differential is measured and fed back to the controller, which adjusts the servovalve command signal based on both the position

and delta pressure feedbacks. The delta pressure feedback is also used to limit the oil column resonance effects, thus explaining the common reference to the delta pressure gain as "numerical damping."

We next turn to the modeling of the complete system response. Each of the subsystems with its governing equation is described below.

$$1. \text{ Controller: } V_c(s) = H_c(s)[x_c(s) - x_s(s)] - H_{dp}(s)\Delta P(s) \quad (18a)$$

As indicated in Eq. (18a) and Fig. 3, the error between the commanded shaker input motion x_c and the position feedback (the actual position of the moving mass, x_s), as well as the delta pressure signal (pressure differential), are used by the controller to adjust the servovalve command signal V_c . $H_c(s)$ and $H_{dp}(s)$ denote the transfer functions of the controller and delta feedback loop, respectively.

$$H_c(s) = K_p + K_d \frac{s}{s + p_1} \quad (18b); \quad H_{dp}(s) = K_{dp} \frac{s}{s + p_2} \quad (18b)$$

Eq. (18b) represents a controller model that is referred to as the lead compensator approximation of a proportional-derivative (PD) conditioned control scheme [7]. The PD control is usually adopted to reduce the rise-time and the overshoot of the system response, but pure derivative control is not practical because of the amplification of sensor noise by differentiation and should be approximated by lead compensator form [7]. In Eq. (18b), the transfer function for the delta pressure loop is expressed as another lead compensator approximation for same reason as in the PD control. In Eqs. (18), ΔP is the differential pressure across the actuator piston, and K_p , K_d , K_{dp} denote the proportional, derivative, and delta-pressure control gains, respectively. K_d and K_{dp} are not exactly identical to conventional derivative gain and delta pressure gain. The lead compensation approaches pure PD control when a large value is used for the constant p_1 or p_2 . Constants p_1 and p_2 designate the pole location of each transfer function. These control gains and constants p_1 and p_2 affect the closed loop response of the system, and are generally determined by trial and error until the target performance criteria are achieved.

$$2. \text{ Servovalve: } q(s) = k_q e^{-\tau s} V_c(s) \quad (19)$$

Eq. (19) describes the oil flow rate into the actuator pressure chamber (q) that is generated by the servovalve in response to the servovalve command signal (V_c) [6]. A linear relationship between q and V_c is assumed, with the constant of proportionality being the flow gain coefficient (k_q), which is a characteristic of the three-stage servovalve used. While a three-stage servovalve consists of both an outer and inner feedback loop, the inner control loop was neglected since servovalve control is significantly more accurate than that of the other subsystems [6]. The time delay (τ) in Eq. (19) is included to model the time necessary to overcome the mechanical and hydraulic inertia of the servovalve.

$$3. \text{ Actuator: } q(t) - A\dot{x}_s(t) = k_{le}F(t) + \frac{V}{4\beta A}\dot{F}(t) \quad (20)$$

Eq. (20) is the flow continuity equation that converts the oil flow rate (q) into piston motion (\dot{x}_s) and actuator forces (F) [3, 6]. The oil flow rate (q) delivered through the servovalve produces a volume change in the actuator pressure chamber, thereby inducing piston movement. However, oil leakage through piston seals and oil compressibility result in additional oil volume changes that must be compensated for by the oil flow rate, thereby reducing the net flow rate as expressed by Eq. (20). In the above equation, $F(t)$ is the force acting across the actuator, V is the effective volume of both chambers of the actuator cylinder, A is the effective piston area, β is the bulk modulus of the fluid, and k_{le} is the leakage coefficient associated with the piston seals.

4. Structure: Equation of motion is Eq. (2) with external force vector taken as $\underline{f}(t)$ in Fig. 1(b).

From the above equations, the transfer function, $H_{CSI}(s)$, describing the overall system relationship between the commanded (input) position, x_c , and the absolute actuator position achieved by the linear shaker, x_{sa} , can be derived using the transfer function of the servovalve-actuator subsystem, $H_s(s)$, and the transfer function of the MDOF test structure, $H_B(s)$. This transfer function is referred to herein as the total transfer function of the linear shaker–test structure system, and is given as,

$$H_{CSI}(s) = \frac{x_{sa}(s)}{x_c(s)} = \frac{H_s(s)H_C(s)k_t e^{-\tau s}}{1 - H_B(s) + H_s(s)k_t e^{-\tau s} \left[H_C(s)(1 - H_B(s)) + s^2 \left(\frac{m_s}{A} H_{dp}(s) \right) \right]} \quad (21)$$

$H_s(s)$ describes the relationship between the servovalve output (flow rate, q) and the actuator relative displacement (x_s); therefore it depends on actuator and structural parameters as,

$$H_s(s) = \frac{x_s(s)}{q(s)} = \frac{1 - H_B(s)}{s^3 \left(\frac{V m_s}{4 \beta A} \right) + s^2 m_s k_{le} + sA(1 - H_B(s))} \quad (22)$$

The transfer function $H_B(s)$ is derived from the building's equations of motion, Eq. (2), taking the absolute displacement of the moving mass (x_{sa}) as input and the roof displacement (x_n) as output, assuming that the linear shaker is installed at the roof level.

$$H_B(s) = \frac{x_n(s)}{x_{sa}(s)} = - \sum_{i=1}^N \frac{\phi_{in}^2 m_n}{M_i} \frac{s^2}{s^2 + 2\zeta_i \omega_i s + \omega_i^2} \quad (23)$$

where

ϕ_{in} = n -th (or roof) component of the i -th vibration mode shape

M_i, ζ_i, ω_i = Modal mass, modal damping, and natural circular frequency of i -th mode.

NUMERICAL EXAMPLE

The two motion transformation solutions presented above (the transfer function and least squares methods) including the CSI effects are illustrated through a numerical example using the three-story, two-bay planar frame shown in Fig. 4. The first three natural frequencies of the example building are 2.85Hz, 9.26Hz and 16.4Hz, respectively. We assumed damping ratios of 5% for all the modes, and that the linear shaker was attached to the roof as shown in Fig. 4. The 1940 El Centro N-S acceleration history, with acceleration values multiplied by 0.15, was used as the control motion. Amplitude scaling was performed to match the performance specifications of the UCLA NEES linear shaker, which has 22.25 kN (5 kips) moving mass and the dynamic actuator of the following nominal capacities: 66.75 kN (15 kips) maximum force, ± 38.1 cm (± 15 inch) stroke, and 340.7 lpm (90 gpm) peak flow capacity.

Using the transfer function method, four different motion transformations were performed to match the displacement responses of the first, second and third stories, as well as the inter-story drift between the second and third floors. From Eq. (9), filters for each response quantity match were derived. For example, filter $T_3(s)$, which equates the roof displacement response for base and top excitation cases can be expressed as,

$$T_3(s) = \frac{H_{31}(s)m_1 + H_{32}(s)m_2 + H_{33}(s)m_3}{m_s H_{33}(s)} \quad (24)$$

The filters $T_1(s)$ and $T_2(s)$ to match the 1st and 2nd floor displacements, respectively, can be derived similarly. To match inter-story drift between roof floor and 2nd floor (i.e., $\Delta_{32} = x_3 - x_2$), Eq. (9) was modified to,

$$T_{32}(s) = \frac{m_1(H_{31}(s) - H_{21}(s)) + m_2(H_{32}(s) - H_{22}(s)) + m_3(H_{33}(s) - H_{23}(s))}{m_s(H_{33}(s) - H_{23}(s))} \quad (25)$$

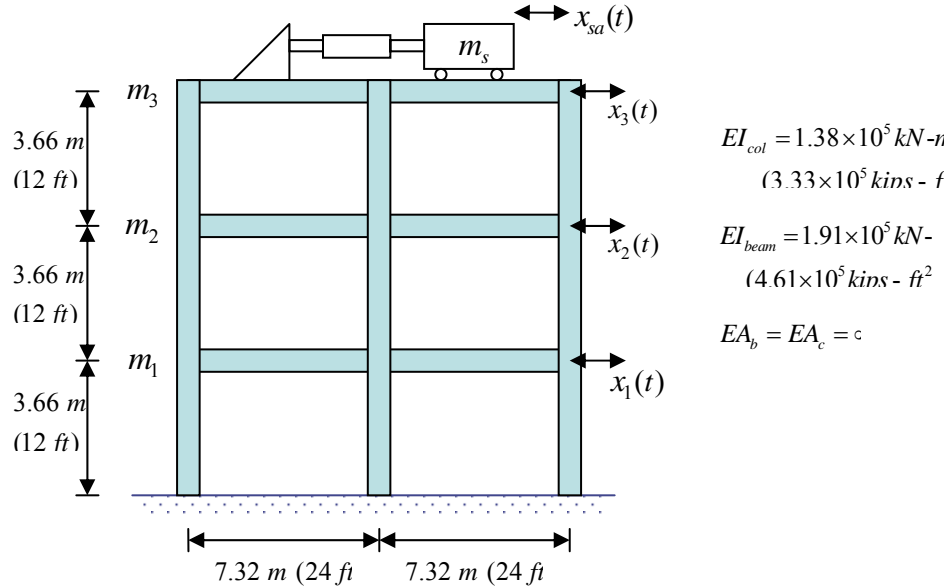


Fig. 4. Three-story, two-bay example building

Fig. 5 shows the amplitude and phase spectra of filter $T_3(s)$. As shown in Fig. 6, the transfer function method yields excellent agreement (as expected) between the top and base excitation cases for the target response quantity and minor discrepancies for non-target response quantities such as the 1st and 2nd story displacement. The discrepancy between the top and base excitation responses, herein termed the motion transformation error, can be quantified using a normalized root mean square (RMS) tracking error, defined as:

$$\text{Normalized RMS tracking error} = \frac{\sum_{i=1}^N \sqrt{(y'_i - y_i)^2}}{\sum_{i=1}^N \sqrt{y_i^2}} \quad (26)$$

where the summation occurs over time and y and y' denotes generic response quantities for base and top excitations, respectively (e.g., $y, y' = x_n, x'_n$ for roof displacement response).

Table 1 presents a summary of normalized RMS tracking errors for motion transformations using the Transfer Function method and Least Squares method. For the transfer function method, the target floor response quantities should theoretically be a perfect match with the base excitation response (RMS error = 0); however, non-zero RMS errors were computed due to numerical errors associated with the discrete Fourier/Laplace transformations. Values in the parenthesis represent relative displacement or relative acceleration to its lower floor, i.e., Roof-2nd floor relative displacement, 2nd-1st floor relative displacement, etc. from the top. When a local response quantity such as inter-story drift is matched, relatively large discrepancies are observed on global response quantities (floor responses). For buildings with non-uniform mass or stiffness distributions, the non-target response quantity errors would likely be greater. The least squares procedure modifies the control motion such that the top-down and bottom-up responses are matched in an average sense in terms of displacement, velocity and acceleration at selected degrees-of-freedom. Using Eq. (17), a single transformation was performed for the example structure to

modify the control motion to simultaneously match as closely as possible all three story displacement, velocity and acceleration responses. Fig. 7 shows the displacement responses obtained using the least squares method. The least squares method generally minimizes the RMS errors for any particular degree-of-freedom as effectively as the transfer function method. However, the least squares method has the advantage of having consistently small tracking errors for all three degrees-of-freedom.

Table 1. Normalized RMS tracking errors for each motion transformation

	TFM (x_1 match)	TFM (x_2 match)	TFM (x_3 match)	TFM (Δ_{32} match)	Least Squares Method
Roof Displ.	0.143	0.082	0.001	0.389(0.001)	0.043
2nd Floor Displ.	0.077	0.042	0.126	0.528(0.442)	0.040
1st Floor Displ.	0.042	0.108	0.246	0.636(0.636)	0.116
Roof Accel.	0.913	0.510	0.002	1.094(0.009)	0.232
2 nd Floor Accel.	0.165	0.056	0.698	1.499(1.267)	0.138
1st Floor Accel.	0.074	0.801	1.292	1.700(1.700)	0.292

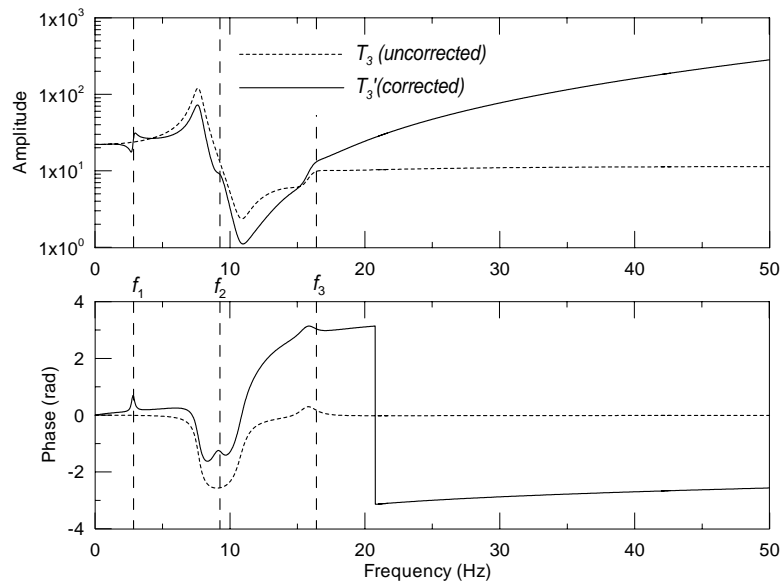


Fig. 5. Comparison of amplitude and phase spectra of filter that includes CSI effects (T_3') and that neglects CSI effect (T_3), Transfer Function Method

At this point, it is important to distinguish the different types of errors associated with applying the LSSS test method. The above motion transformation procedure illustrates how a control earthquake ground motion can be modified such that the LSSS testing method replicates the base excitation response with reasonable accuracy assuming perfect actuation. The difference between the base and top excitation responses can be termed the motion transformation error, and can be attributed to the different inertial force distributions between the base and top excitation cases. However, due to the CSI effects resulting from the dynamic coupling between the actuator and the test structure, the assumption of perfect actuation is not valid for most cases. The difference between the expected (command) and achieved force outputs in the piston is herein termed the actuation error. Unlike the motion transformation error, the actuation error can be pre-compensated for in the shaker command signal. The pre-compensation can be addressed using an analytical model, although model improvements based on forced-vibration testing could be implemented.

Each of the filters, which were previously derived using the transfer function method assuming perfect actuation (e.g., T_1 , T_3 , T_{32}), were pre-corrected for CSI effects using $H_{CSI}(s)$. For example, $T_3'(s)$ is the CSI-corrected filter that will compensate for the actuation error:

$$T_3'(s) = [H_{CSI}(s)]^{-1} T_3(s) \quad (27)$$

Fig. 5 shows the amplitude and phase spectra of the uncorrected filter $T_3(s)$ and CSI-corrected filter $T_3'(s)$. Similarly, the shaker input motion derived using the least squares method, Eq. (17), can also be corrected in the frequency domain using $H_{CSI}(s)$. Fig. 5 was plotted using control gains determined for the UCLA NEES linear shaker system installed on a stationary base.⁵

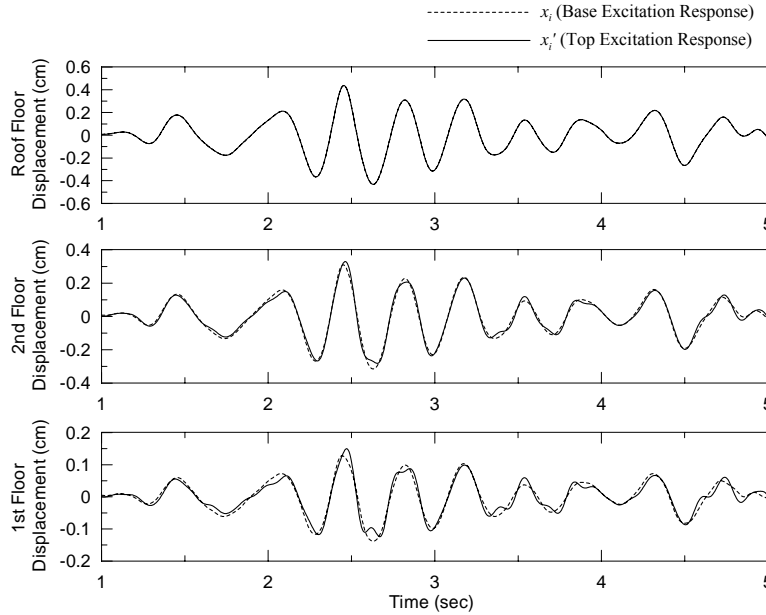


Fig. 6. Comparison of base and top excitation roof displacement responses using the Transfer Function Method (using $T_3(s)$) ; assuming perfect actuation

The building displacement response from the input derived using the transfer function filter T_3 without correcting for CSI effects are compared with the target responses (base excitation, dashed lines) in Fig. 8. As shown in the figures, the errors due to the neglect of CSI effects consist largely of phase differences, although some amplitude differences are also present. The observed differences between the achieved and target building responses in Fig. 8 result from the imperfect actuation and motion transformation. When the shaker input motion is corrected for CSI effects, the top excitation responses (solid lines) in Fig. 8 are the same as the top excitation responses (solid lines) in Fig. 6. Since the actuation error can be pre-compensated to the extent that the linearized model is valid, any remaining discrepancies between the top and base excitation cases would be associated with the motion transformation and epistemic errors (due to modeling uncertainty associated with the shaker and structural systems) once the input motion is CSI-corrected.

⁵ Optimal control gains are case-dependent, since the total transfer function of the linear shaker-structure system $[H_{CSI}(s)]$ is dependent on the hydraulic system parameters as well as the structural parameters of test structure. Values of the control gains and constants used in this paper are as following; $K_p = 0.472$ V/cm (1.2 V/in), $K_d = 0.591$ V/s/cm (1.5V/s/in), $K_{dp} = 3.231 \times 10^{-2}$ V/MPa (2.229×10^{-4} V/psi), $p_1 = 1/0.02$ rad/s, $p_2 = 1/0.07$ rad/s. The time delay and leakage coefficients were not considered, since the simulation model ignoring these terms shows good results when compared to the test data. The time delay(τ) and leakage coefficient(k_{le}) were set to zero in this model.

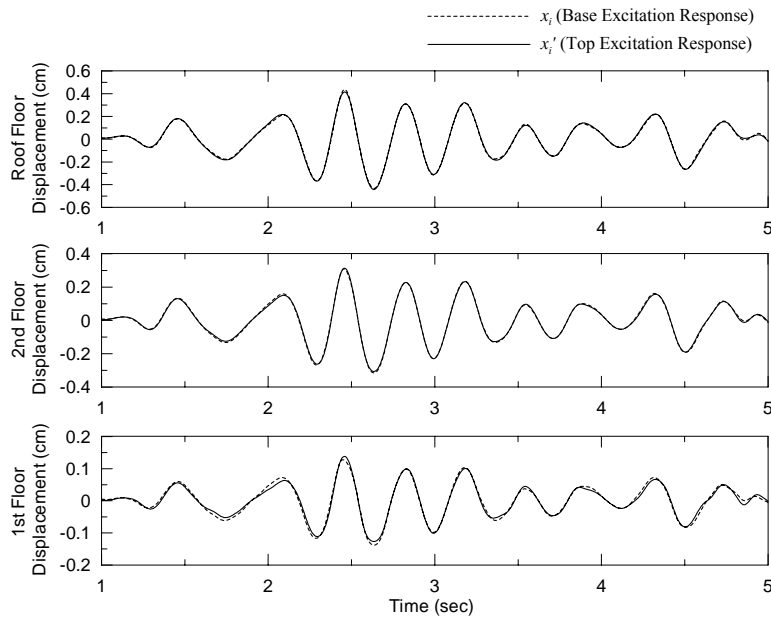


Fig. 7. Comparison of base and top excitation displacement responses using the Least Squares Method; assuming perfect actuation

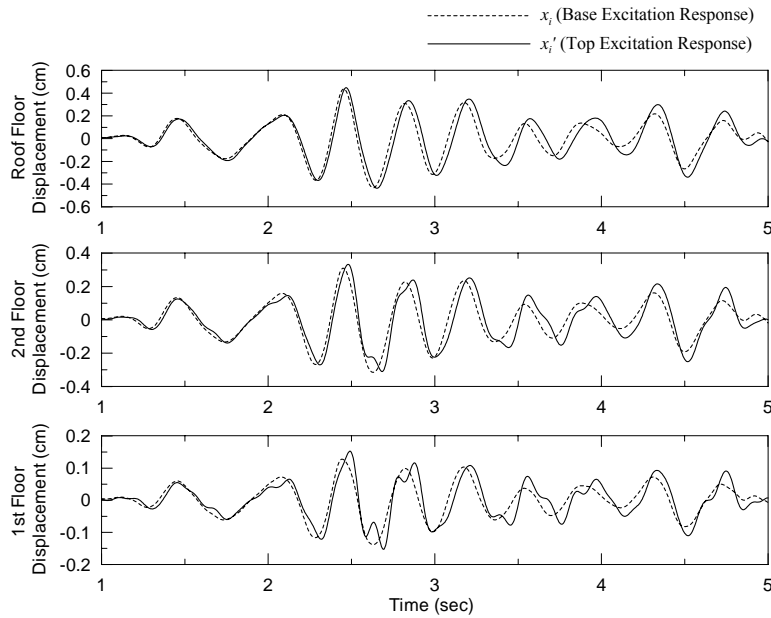


Fig. 8. Comparison of base and top excitation roof displacement responses using the Transfer Function Method (using $T_3(s)$) from uncorrected (for CSI effects) input
DESCRIPTION OF THE NEES@UCLA LINEAR INERTIAL SHAKER

The nees@UCLA Linear Inertial Shaker is driven by a hydraulic actuation system capable of moving a nominal weight of 22.25 kN (5 kips) with a peak force of 66.75 kN (15 kips) through a stroke of ± 38.1 cm (± 15 inch). The system utilizes two 10-gallon accumulators in the pressure-side charged to 3000 psi and two return-side accumulators charged to 150 psi. The flow through the actuator is varied using a

three-stage MTS servovalve (model no: 256.09.A02) with 340.7 lpm (90 gpm) peak flow capacity and a 3 dB roll-off at approximately 90 Hz.

The linear shaker has two operational modes, namely, a displacement mode and an acceleration mode. A Baluff sensor with a $\pm 10V$ output for a displacement range of ± 40.64 cm (± 16 inches) provides displacement feedback, while a PCB accelerometer (model no. 3703G2FD3G) with a sensitivity of 1 g/V and a range of 5g mounted on the side of the base of the moving mass provides acceleration feedback. In addition, a delta-pressure sensor is used to close a differential pressure loop to damp out the oil-column resonance for displacement control as described in the previous section. The system also has a load cell to measure the force transmitted to the structure and a GPS module to provide time stamping for synchronization with external data acquisition systems.

In the displacement mode, the user can choose one of three control algorithms: PD, Optimal (LQG) and Adaptive (ARMAKOV tracking). The PD control algorithm is of a standard form described in the previous section and the nominal transfer function of the controller as given by Eqs (18). The optimal control algorithm uses the Linear-Quadratic-Gaussian (LQG) design approach [8]. The system is represented in linear state-space form and a quadratic cost function based on the tracking error and the control signal is minimized with respect to the controller parameters. The state space representation of the system is obtained using a subspace based system identification approach known as N4SID [9], and the states of the system are estimated from the sensor measurements using a Kalman filter [8]. The optimal control algorithm provides a flat frequency response over a larger bandwidth than the PD controller. The adaptive controller [10] compensates for gain and phase errors in sinusoidal tracking by pre-compensating the command to the PD controller. Tracking errors of less than 2% for earthquake profiles are typical in the displacement mode.

In the acceleration mode, the user can choose to use the optimal controller with or without adaptive pre-compensation. The design approach for the optimal and adaptive controllers is the same as for displacement control. The tracking errors in the acceleration mode are higher than in the displacement mode because of friction and the excitation of structural modes of the shaker.

The control algorithms are implemented on a fully digital dSPACE real-time system based on a DS1103 controller board. The board uses a Power PC 604e 400 MHz processor and has 16 16-bit analog-to-digital (A/D) converters, 4 12-bit A/Ds, 8 14-bit digital-to-analog (D/A) converters, 32 bits of digital inputs/outputs, and other I/O features. The sensor signals are fed to the 16-bit A/Ds through integrated anti-aliasing signal conditioning and the current command is sent to the servovalve driver from a D/A channel. All inputs and outputs are optically isolated to protect the control system from voltage spikes induced by operating in a potentially noisy environment. The control algorithms are run at a sample rate of 5 KHz and are implemented as Simulink models. With the dSPACE interface to Simulink, the Real-Time Interface (RTI), code is automatically generated for the model, built, and implemented on the real-time hardware. Simulink is the graphical simulation environment of Matlab.

The user operates the system using a Graphical User Interface (GUI) built in dSPACE's ControlDesk environment and is able to perform all tasks in preparing, running, and monitoring the test. Some of these tasks are selecting control modes, controller types, reference commands, safety checks, monitoring GPS operation status, and acquiring data for post processing. A requirement for testing is to import recorded earthquake data, preview the time history, scale the signal appropriately and play it as a reference profile for the table to track. This is accomplished using test automation features in the ControlDesk environment. These automation features also allow the user to generate complete test reports containing user identification, test location, test profiles, controller selection, GPS timestamps, acquired sensor data and various other signals. The system architecture is thus well suited to replicate the reference time histories generated by the LSSS method for the purpose of experimental validation.

CONCLUSIONS

The linear shaker seismic simulation (LSSS) method is a new method for forced-vibration testing of structures to induce seismic excitation demands that are consistent with earthquake induced shaking at the structure base. This paper addresses two challenges associated with implementation of the LSSS method in the context of linear elastic seismic response for structures. These challenges consist of (a) identifying a linear shaker input motion which produces a structural response similar to that of the building shaken from the base by an actual earthquake, and (b) pre-correcting the input motion to account for control-structure interaction effects. Procedures for making these corrections have been presented that allow the structural response associated with any particular ground motion response history to be reproduced with top down excitation through a linear shaker accounting for motion transformation and CSI effects.

The potential usefulness of the LSSS method was investigated using numerical simulations of the needs@UCLA linear shaker attached to the roof of a generic three-story test structure. For motion transformation, the 1940 El Centro ground motion was filtered in the frequency domain using the LSSS transfer function approach, as well as in the time domain using the LSSS least squares approach. Analysis results showed that the linear elastic seismic response of low-rise buildings can be replicated with good accuracy once the filtered shaker input motions are pre-compensated for control-structure interaction effects. However, future experimental studies are required to validate this new test method in consideration of unmodeled epistemic and aleatoric uncertainties associated with material properties, servo-hydraulic parameters, and modeling of structural and servo-hydraulic shaker systems. Furthermore, the LSSS testing method should be investigated in the context of nonlinear (material and geometric) seismic response of structures.

REFERENCES

1. Joint Technical Committee on Earthquake Protection, *Earthquake Hazard and earthquake Protection*, Los Angeles, CA, 1993.
2. Dimig J, Shield C, French C, Bailey F, Clark A, "Effective force testing: a method of seismic simulation for structural testing", *J. Structural Engineering*, 1999, ASCE, **125**(9), 1028-1037.
3. Dyke SJ, Spencer BF, Quast P, Sain MK. "Role of control-structure interaction in protective system design", *J. Engineering Mechanics*, 1995, ASCE, **121**(2), 322-338.
4. Shing PB, Mahin SA, "Pseudodynamic test method for seismic performance evaluation: theory and implementation", *EERC Report. UBC/EERC-84/01*, University of California, Berkeley, CA, 1984.
5. Wang YP, Lee CL, Yo TH, "Modified state-space procedures for pseudodynamic testing", *Earthquake Engineering and Structural Dynamics*, 2001, **30**(1), 59-80.
6. Conte JP, Trombetti TL. "Linear dynamic modeling of a uni-axial sero-hydraulic shaking table system", *Earthquake Engineering and Structural Dynamics*, 2000, **29**(9), 1375-1404.
7. Franklin GF, Powell JD, Emami-Naeini A, "Feedback control of Dynamic systems", 4th Edition, Prentice Hall: New Jersey, 2002; 310-315.
8. Franklin GF, Powell JD, Workman ML, "Digital Control of Dynamic Systems", 2nd Edition, Addison-Wesley: Massachusetts, 1990; 430-480.
9. Overschee PV and De Moor B, "A Unifying Theorem for Three Subspace System Identification Algorithms", *Automatica*, 1995, **31**(12); 1853-1864.
10. Venugopal R and Bernstein DS, "Adaptive Tracking Using ARMARKOV/Toeplitz Models," *Proceedings of the American Control Conference*, 1998, 144-148.